Energy Technology
Generation, Conversion, Storage, Distribution
www.entechnol.de

Flexible Organic Photovoltaics with Star-Shaped Nonfullerene Acceptors End Capped with Indene Malononitrile and Barbiturate Derivatives

*Basheer Al-Anesi, Srikanth Revoju, Arto Hiltunen, Riikka Suhonen, Thomas M. Kraft, Maning Liu, Haichang Zhang, Zhifeng Deng, Chiara Fedele, Alex Berdin, Noora Lamminen, G. Krishnamurthy Grandhi, Mari Ylikunnari, and Paola Vivo**

The design and synthesis of three star-shaped nonfullerene (NFA) acceptors, TPA-2T-INCN, TPA-2T-BAB, and TPA-T-INCN, based on a triphenylamine (TPA) core and linked through π-conjugated thiophene (T) spacers to different terminal units (3-oxo-2,3-dihydro-1H-inden-1-ylidene) malononitrile, INCN, and 1,3-dimethylbarbituric acid, BAB), are reported. These materials are blended with the widely used poly(3-hexylthiophene-2,5-diyl) (P3HT) donor polymer and tested in flexible organic photovoltaics (OPVs). The NFAs capped with the strong electron-withdrawing INCN unit perform best in OPVs. Both P3HT:TPA-T-INCN and P3HT:TPA-2T-INCN blends also show the highest photoluminescence quenching efficiency (95.8% and 92.6%, respectively). Surprisingly, when reducing the number of T spacers from 2 to 1, the solubility of the NFAs in *o*-dichlorobenzene increases, leading to easier processing during the OPV fabrication and better surface morphology. This explains the best performance of TPA-T-INCN-based blends in OPVs, with a champion power conversion efficiency of 1.13%.

1. Introduction

Organic photovoltaics (OPVs) are an emerging third-generation class of solar cells that have proven to be an advantageous PV harvesting method due to their potential low cost, flexibility, lightweight, and color tunability, combined with simple and scalable manufacturing.[1–3] The active layer of OPVs usually consists of an electron donor and electron acceptor, which are blended together to form a so-called bulk heterojunction (BHJ) structure. Normally, the electron donor is a *p*-type conjugated polymer while the electron acceptor is an n-type fullerene or nonfullerene derivative.[4–6] In recent years, research on nonfullerene acceptors (NFAs) has been strongly intensified as they enable overcoming the critical disadvantages of fullerene-based acceptors, such as the complex syntheses, poor light absorption properties, limited tunability of the energy levels, and chemical instability.[7–10] A variety of donor polymers has been blended with the numerous NFA proposed designs, with poly(3-hexylthiophene) (P3HT) being one of the most commonly reported donors.[4,11–15] Linear-shaped π-conjugated acceptor (A)—donor (D)—acceptor (A) structures are among the most extensively investigated NFAs.[16–19] On the other hand, 1D linear-shaped structures exhibit anisotropic optical and electrical properties, thus posing a challenge for the development of high-performance devices.[20–25] The development of star-shaped NFAs offers a possible solution to the drawbacks of linear NFAs. Star-shaped A–π–D–π–A NFAs consist of a central donor core linked to several linear chains arranged in a 3D geometry.[26–28] In contrast to their linear analogs, star-shaped NFAs ensure 1) tunability of the lower unoccupied orbital levels (LUMO) through modification of the acceptor units, with a direct effect on the open-circuit voltage (V_{OC}) of the corresponding OPVs; 2) possible broadening of the absorption spectrum (and thus improved solar absorption) up to

B. Al-Anesi, S. Revoju, A. Hiltunen, M. Liu, C. Fedele, A. Berdin, N. Lamminen, G. K. Grandhi, P. Vivo
Faculty of Engineering and Natural Sciences
Tampere University
33014 Tampere, Finland
E-mail: paola.vivo@tuni.fi

The ORCID identification number(s) for the author(s) of this article can be found under https://doi.org/10.1002/ente.202200264.

DOI: 10.1002/ente.202200264

R. Suhonen, T. M. Kraft, M. Ylikunnari
VTT Technical Research Centre of Finland
90571 Oulu, Finland

H. Zhang
Key Laboratory of Rubber-Plastics of Ministry of Education/Shandong Province (QUST)
School of Polymer Science and Engineering
Qingdao University of Science and Technology
Qingdao 266042, P. R. China

Z. Deng
National and Local Joint Engineering Laboratory for Slag Comprehensive Utilization and Environmental Technology
School of Material Science and Engineering
Shaanxi University of Technology
Hanzhong 723001, P. R. China

the near-infrared region; and 3) minimization of the molecular aggregation and enhancement of the exciton dissociation due to the 3D structures that may lead to high short-circuit current density (J_{SC}) in OPVs.[29–31] For a high-performance star-shaped NFA, choosing the central core and the attached arms is crucial. Triphenylamine (TPA) offers excellent hole transport and electron donation properties, and it is widely used as hole-transporting material for perovskite solar cells or organic light-emitting devices.[32,33] Hence, it can serve as the effective central core of a star-shaped NFA. Key examples of TPA-based NFAs have been reported by Lin et al.[11] and Liu et al.[12]. In the study by Lin et al.,[11] the authors designed an NFA molecule with diketopyrrolopyrrole (DPP) arms, which displayed good optical properties, suitable energy levels, and excellent thermal stability. In OPVs, a high V_{OC} of 1.18 V was achieved. Some years later, Liu et al. showed that the replacement of a benzene core with TPA in an NFA design with isoindigo arm leading to more efficient OPVs.[12] Indeed, for benzene- and TPA-core NFAs blended with P3HT donor, the corresponding devices displayed a power conversion efficiency (PCE) of 0.19% and 0.81%, respectively.

Thiophene (T) is also a well-known and readily synthesized electron-rich unit for high-performance organic electronic materials. The incorporation of *T* units between the central covalent core and the terminal electron acceptor unit typically contributes to improving the solubility of the star-shaped molecules as well as the expansion of the π-conjugation system.[34] Recently, Luponosov et al. reported four TPA-based star-shaped small molecules end capped with dicyanovinyl electron-withdrawing groups connected to the core through a varying number of *T* units in the arms (from 0 to 4). The authors found that the length of the π-bridge could significantly affect the highest occupied molecular orbital (HOMO) level and the optical absorption, in turn increasing the performance of the corresponding OPVs.[35] Owing to the A–π–D–π–A structure of star-shaped molecules, LUMOs are primarily located at the electron-acceptor terminal units, while HOMOs tend to occupy the electron-donating central core units. Consequently, the selection of the electron-acceptor terminal units enables the tuning of optical absorption in the long-wavelength range and the adjustment of the LUMO level to maximize the V_{OC}.[29] Thus, the acceptor groups in the star-shaped molecules play a crucial role for high-performing OPVs. In the past few years, (3-oxo-2,3-dihydro-1H-inden-1-ylidene)malononitrile (INCN) electron-withdrawing unit was widely used in the design of NFA materials, the most popular INCN-based NFA being ITIC.[36] Recently, Bo's group designed linear-shaped materials, whose ends were both capped with INCN acceptor units. Using the molecule as NFAs in OPVs led to a PCE up to 12.04%.[37] The introduction of 1,3-dimethylbarbituric acid (BAB) electron-accepting unit enabled the effective adjustment of the lowest unoccupied molecular orbital (LUMO) in NFAs.[38,39] However, to the best of our knowledge, molecules combining TPA core, *T* bridge, and INCN or BAB moieties as electron-withdrawing capping ends in the same material are yet to be reported. Herein, we pioneered the syntheses of NFAs with A–π–D–π–A configuration, TPA-2T-INCN and TPA-2T-BAB, in which electron-withdrawing INCN or BAB groups are connected to TPA through two *T* spacers, respectively. Alkyl side chains are added to both TPA-2T-INCN and TPA-2T-BAB to increase the solubility of the NFAs in nonpolar organic solvents. Upon blending with P3HT donor, the NFAs were tested in the active layer of flexible organic solar cells. The INCN-based blends appeared more promising than the BAB-based analogs, although the very modest PCE values were related to the low J_{SC} values, as the solubility of the NFAs in the typically used *o*-dichlorobenzene solvent was rather limited. Furthermore, when reducing the number of *T* spacers (from 2 to 1) in the molecule TPA-T-INCN, we achieved increased solubility that eased processing during OPV fabrication. Indeed, TPA-T-INCN in P3HT blends led to the most efficient OPV (PCE = 1.13%) as a result of the increased J_{SC} and FF. These findings could be partially explained by the reduced aggregation in the solid state for TPA-T-INCN compared with the other NFAs, as suggested by our theoretical study. Finally, the morphological analysis of the blends and the interfacial charge transfer dynamics study further support the superior performance of P3HT:TPA-T-INCN-based OPVs.

2. Results and Discussion

2.1. Synthesis

The chemical structures of three new star-shaped NFA molecules, namely, TPA-T-INCN, TPA-2T-INCN, and TPA-2T-BAB, are shown in **Figure 1**. The materials were synthesized according

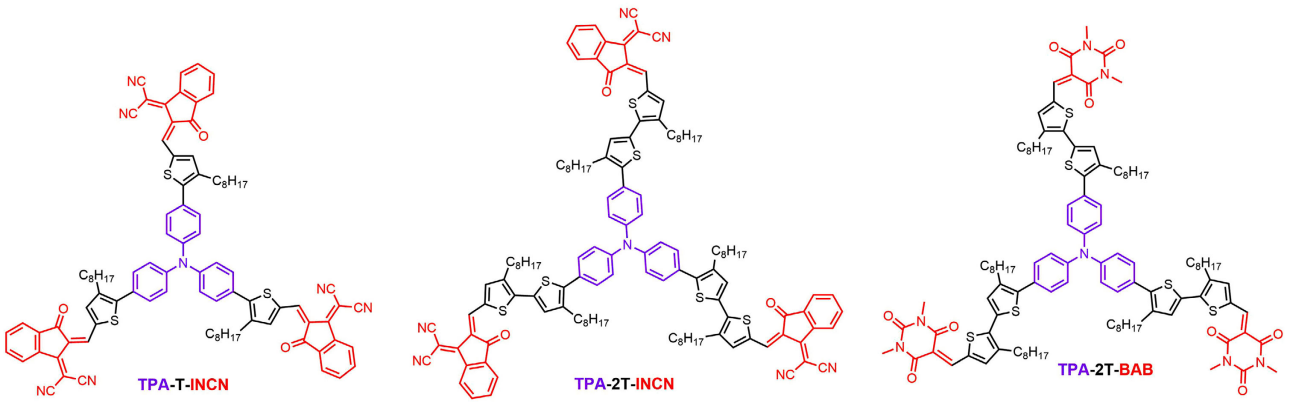

Figure 1. Chemical structures of TPA-T-INCN, TPA-2T-INCN, and TPA-2T-BAB star-shaped NFAs.

to Scheme S1, Supporting Information. The reaction intermediates were prepared by following a literature procedure.[40] Compound TPA reacted with *T* or 2*T* under palladium-mediated Suzuki coupling reaction conditions to prepare the intermediate compounds TPA-T or TPA-2T. Subsequently, Knoevenagel condensation of TPA-T or TPA-2T with 3-(Dicyanomethylidene) indan1-one or 1,3- Dimethylbarbituric acid resulted in the target molecules TPA-T-INCN, TPA-2T-INCN, and TPA-2T-BAB with a yield of 83%, 85%, and 90%, respectively. The synthetic procedures and fundamental chemical analyses are thoroughly presented in Supporting Information.

2.2. Optical and Electrochemical Properties

The UV–vis absorption spectra of the star-shaped NFAs in solution (solvent is distilled dichloromethane) and film state (spin-coated films of NFAs and their blends with, P3HT, donor) are depicted in **Figure 2**. The corresponding optical data are summarized in **Table 1**.

As shown in Figure 2a, TPA-T-INCN solution absorbs between 350 and 700 nm with the first exciton peak at 563 nm. The UV absorption peaks in the short-wavelength region correspond to the $\pi - \pi^*$ transition and the ones in the longer wavelength region can be attributed to the intramolecular charge transfer (ICT) transition between the TPA-thiophene electron-donating and electron-withdrawing INCN units.[41] As shown in Figure 2a,b, by increasing the number of thiophene spacers (from TPA-T-INCN to TPA-2T-INCN), the absorption is red-shifted due to the extended conjugation.[42] Consequently, the first exciton peak of TPA-2T-BAB shows a blueshift compared with those of the other two NFAs, that is, at 491 nm. The enhanced absorption in the blue region upon the replacement

Table 1. Optical and electrochemical properties of the target NFAs in solution and film phase. The wavelength corresponding to the first exciton peak is denoted as $\lambda_{abs,exciton}$.

NFA	$\lambda_{abs,exciton}$ (solution)	$\lambda_{abs,exciton}$ (film)	λ_{onset} [a)]	E_g^{opt} [b)]	E_{HOMO} [c)]	E_{LUMO} [c)]	E_g^{DPV} [d)]
	[nm]	[nm]	[nm]	[eV]	[eV]	[eV]	[eV]
TPA-T-INCN	563	575	643	1.93	−5.4	−3.6	1.8
TPA-2T-INCN	488	665	726	1.71	−5.2	−3.6	1.6
TPA-2T-BAB	491	498	595	2.08	−5.2	−3.2	2.0

[a)]Long-wavelength onset of absorption, λ_{onset}, from the absorption spectrum in solution; [b)]Optical bandgap, E_g^{opt}, calculated from the absorption onsets; [c)]$E_{HOMO/LUMO}$ energy was calculated from DPV voltammograms: $-E_{HOMO/LUMO} = E_{onset(ox)/(red)} + 4.8$eV, where $E_{onset(ox)/(red)}$ is the onset potential for the oxidation/reduction versus ferrocene internal standard; [d)]Electrochemical bandgap estimated from the DPV data.

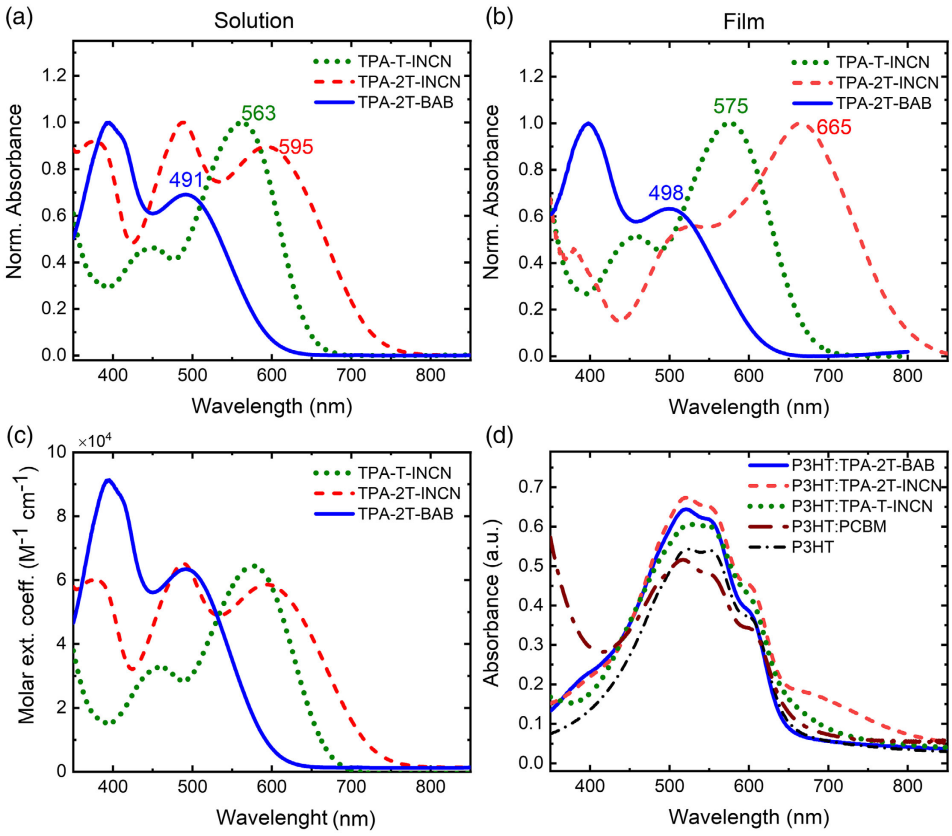

Figure 2. Normalized UV–vis absorption spectra of NFAs: a) solution and b) corresponding film. c) Extinction coefficients of NFAs, calculated based on the corresponding absorption spectra in (a). d) UV–vis absorption spectra of thin-film NFAs blended with P3HT donor polymer (the same ratio between P3HT and NFA was used for comparison). The absorption of P3HT film and P3HT:PCBM blend is also included for comparison.

of INCN with BAB groups is explained by the lower electron-withdrawing ability of TPA-2T-BAB, which is in agreement with the differential pulse voltammetry (DPV) data presented in Table 1. Indeed, from DPV analysis, the highest LUMO level (−3.2 eV) is achieved for TPA-2T-BAB NFA, confirming it as the weakest electron acceptor. The LUMO trend for the NFAs (Table 1) also helps explaining the superiority of INCN-based solar cells over the ones containing TPA-2T-BAB in the active layer (see Section 2.4). The optical bandgaps (E_g) are 1.93, 1.71, and 2.08 eV for TPA-T-INCN, TPA-2T-INCN, and TPA-2T-BAB, respectively, as determined from their absorption onsets. The values are quite comparable with the E_g calculated from the DPV data (see Table 1). We further calculated the molar extinction coefficients (Figure 1c) for each NFA based on the corresponding absorption spectra in the solution phase (Figure 1a). It is noted that only TPA-2T-BAB exhibits a relatively low extinction coefficient at lower energies compared with the other two cases, which further supports the low electron-withdrawing ability of this material.

As shown in Figure 2b, the absorption spectra of TPA-T-INCN and TPA-2T-INCN films are remarkably redshifted compared with the corresponding spectra of the materials in the solution phase. This may indicate J-aggregation of adjacent molecules in the solid state, which enables us to harvest more photons in the near-infrared region (NIR).[43] TPA-2T-INCN exhibits the most pronounced redshift of 70 nm among the studied NFAs (see Table 1). On the other hand, TPA-2T-BAB displays negligible changes in its absorption spectrum when switching from the solution to the film form, suggesting negligible molecular aggregation in the solid state. The lower degree of aggregation in TPA-2T-BAB and TPA-T-INCN compared with TPA-2T-INCN can be explained at molecular level by our density functional theory (DFT) study (details in Supporting Information). The additional thiophene unit in the branch backbone induces a high degree of coplanarity and a small twisting angle (3.89° for TPA-T-INCN, 0.37° for TPA-2T-INCN, and 0.05° for TPA-2T-BAB, Figure S5, Supporting Information) between the donor unit (i.e., thiophene) and the acceptor (INCN or BAB). This might be caused by the higher flexibility of the side chain due to the additional thiophene units. Pursuing a high degree of coplanarity of the branch chain is beneficial for promoting the intra- and intermolecular charge transport.[44–47] On the other hand, coplanarity may easily induce J-type aggregation.[48,49] A significant aggregation in the solid state can negatively influence the performance of these NFAs in photovoltaics (see Section 2.4), as expected based on earlier reports.[50,51] The films of TPA-T-INCN, TPA-2T-INCN, and TPA-2T-BAB blends with P3HT exhibit a wide absorption between 350 and 650 nm (Figure 2d). In the case of TPA-T-INCN and TPA-2T-INCN blend films, the absorption extends till 700–800 nm, with the P3HT:TPA-2T-INCN sample showing the highest absorbance in this region (see Figure 2d). The absorption spectrum of TPA-2T-BAB overlaps with that of P3HT. As a result, no broadening of the absorption is observed for the P3HT:TPA-2T-BAB film. When comparing the absorption spectra of P3HT:PBCM, P3HT:TPA-2T-INCN, and P3HT:TPA-2T-BAB blends (all in the same donor:acceptor ratio, Figure 2d), we note that NFA-based blends absorb more light than P3HT:PCBM counterpart, particularly between 455 and 620 nm. This suggests that these new NFAs could potentially lead to OPVs with higher J_{SC} than the widely adopted fullerene derivative (PCBM).

2.3. Interfacial Charge Transfer Dynamics

We studied the charge transfer at the interface between P3HT and the different NFAs by conducting steady-state photoluminescence (PL) and time-resolved PL (TRPL) measurements. **Figure 3**a compares the PL spectra of pristine P3HT film and P3HT:NFA blend films with that of reference P3HT:PCBM blend film. All the samples exhibit the characteristic PL peak at about 725 nm due to the conjugated π-system.[52] A clear PL quenching effect was observed for all P3HT:electron acceptors blend films, revealing that the charge transfer occurs between P3HT and NFAs or PCBM in the bulk heterojunction. The PL quenching efficiencies, calculated by comparing the PL amplitudes with that of the pristine P3HT film, are 75.9%, 92.6%, and 95.8% for the blend films with TPA-2T-BAB, TPA-2T-INCN, and TPA-T-INCN (see **Table 2**), respectively, which are lower than that (98.1%) for the reference

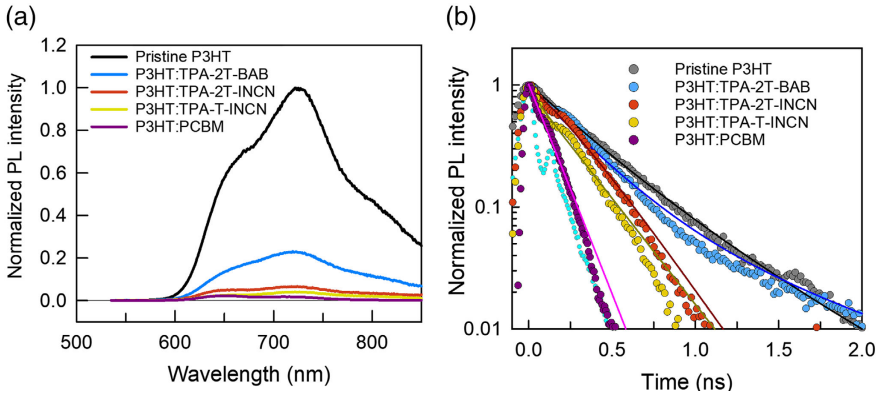

Figure 3. a) Steady-state PL spectra (excitation at 515 nm) and b) TRPL decays (samples excited at 483 nm and monitored at 720 nm) of pristine P3HT film, reference P3HT:PCBM (20:20 mg mL^{-1}) blend film, and P3HT:NFA (15:10 mg mL^{-1}) blend films with TPA-T-INCN, TPA-2T-INCN, and TPA-2T-BAB. Instrument response file (IRF) in cyan color is also included in (b). Solid lines show the fitting results with a biexponential function: $I(t) = A_1 \times \exp(-t/\tau_1) + A_2 \times \exp(-t/\tau_2)$. All measurements were conducted in ambient conditions.

Table 2. PL properties of pristine P3HT film and P3HT:NFA (15:10 mg mL^{-1}) blend films.

Film	PL quenching efficiency [%]	A_1 [%]	τ_1 [ps]	A_2 [%]	τ_1 [ps]	τ_{AVG}[a)] [ps]
Pristine P3HT	–	32	297.8	68	552.4	500.8
P3HT:PCBM	98.1	51.5	126.9	48.5	132.5	129.7
P3HT:TPA-T-INCN	95.8	50.6	134.5	49.4	187.6	165.1
P3HT:TPA-2T-INCN	92.6	64	231.1	36	241.8	238.1
P3HT:TPA-2T-BAB	75.9	87	279.1	13	830.9	448.7

a) $\tau_{AVG} = \frac{A_1\tau_1^2 + A_1\tau_2^2}{A_1\tau_1 + A_2\tau_2}$.

P3HT:PCBM film. Among all NFAs, the highest quenching efficiencies of TPA-2T-INCN and TPA-T-INCN suggest that the electron affinities (LUMOs of TPA-2T-INCN and TPA-T-INCN: −3.6 eV vs. LUMO of TPA-2T-BAB: −3.2 eV) of these materials enable effective acceptance of the injected electrons from the LUMO level (−2.8 eV) of P3HT. Further understanding of the charge transfer dynamics at the P3HT/NFA interface is acquired via TRPL measurements. The corresponding PL decays are shown in Figure 3b. All the decay curves can be fitted well with a biexponential decay function and the fitting results are summarized in Table 2. We assign the fast component (A_1, τ_1) and the slow component (A_2, τ_2) to the trap-assisted nonradiative recombination and the charge carrier radiative recombination, respectively.[53] The average PL lifetime ($\tau_{AVG} = 500.8$ ps) of the pristine P3HT film in its excited state is comparable with what has been reported earlier.[54] The reference P3HT:PCBM blend film shows the most accelerated PL decay with an average lifetime of 129.7 ps, is corresponding to the highly efficient electron injection efficiency, that is, PL quenching efficiency of 98.1%, leading to the generation of high photocurrent that will be discussed in the following section. For the case of NFAs, the incorporation of TPA-T-INCN into the active layer leads to the shortest lifetimes for both fast ($\tau_1 = 134.5$ ps) and slow ($\tau_2 = 187.6$ ps) decay components compared with the other two cases, suggesting that TPA-T-INCN can indeed promote an efficient charge extraction process, that is, electron transfer, while limiting the charge recombination at the interface. It is noteworthy that the P3HT:TPA-2T-INCN blend film exhibits a PL lifetime ($\tau_{AVG} = 238.1$ ps) longer than that ($\tau_{AVG} = 165.1$ ps) of the P3HT:TPA-T-INCN film, which is consistent with the difference in their PL quenching efficiencies. This is the result of the more favorable hole-blocking ability of TPA-T-INCN (HOMO: −5.4 eV) compared with TPA-2T-INCN (HOMO: −5.2 eV), which is crucial to hinder the interfacial charge recombination.

2.4. Flexible Organic Photovoltaics (OPVs)

The newly designed star-shaped NFAs were tested in BHJ OPVs with P3HT electron donor. The OPV active layers were deposited by spin coating the P3HT:NFA blends under investigation (in o-dichlorobenzene solution) with a subsequent annealing step at a relatively low temperature (120 °C). Hence, we focused on low-cost and easily scalable device fabrication, as it involves an inexpensive donor polymer (P3HT), which is the cheapest and most easily synthesizable on a large scale among the available donors for OPVs.[55] Moreover, the P3HT OPV devices are designed as a proof of concept to provide corroboratory evidence of the photophysics results. When preparing the OPVs, the adopted low annealing temperature enabled the use of ITO-coated polyethylene terephthalate (PET) substrates (see the photographs of representative devices in **Figure 4**b). We fabricated OPVs with the inverted ITO/SnO_2/P3HT:NFA/MoO_3/Ag device architecture (n–i–p), in which tin oxide (SnO_2) and molybdenum trioxide (MoO_3) act as electron and hole transport layers, respectively (ETL and HTL). A reference solar cell was also fabricated by blending P3HT with the standard [6,6]-phenyl-C61butyric acid methyl ester (PCBM) fullerene derivative instead of the NFA. The schematic energy band diagram for all the constituents of our OPVs, with the energy values reported with respect to the vacuum level, is shown in Figure 4a. As known, the compatibility between the energy levels of the donor and acceptor constituents of the BHJ blend is crucial for highly efficient OPVs.[5] Figure 4a shows that the new NFAs are all energetically compatible with P3HT, as well as with the other device components. However, a significant difference between the LUMOs of the various electron acceptors is noted (the highest LUMO value, −3.2 eV, is for TPA-2T-BAB vs. −3.6 eV for TPA-2T-INCN/TPA-T-INCN and −3.9 eV for PCBM). This is a key reason for the significant difference in the performance of the corresponding OPVs, as will be

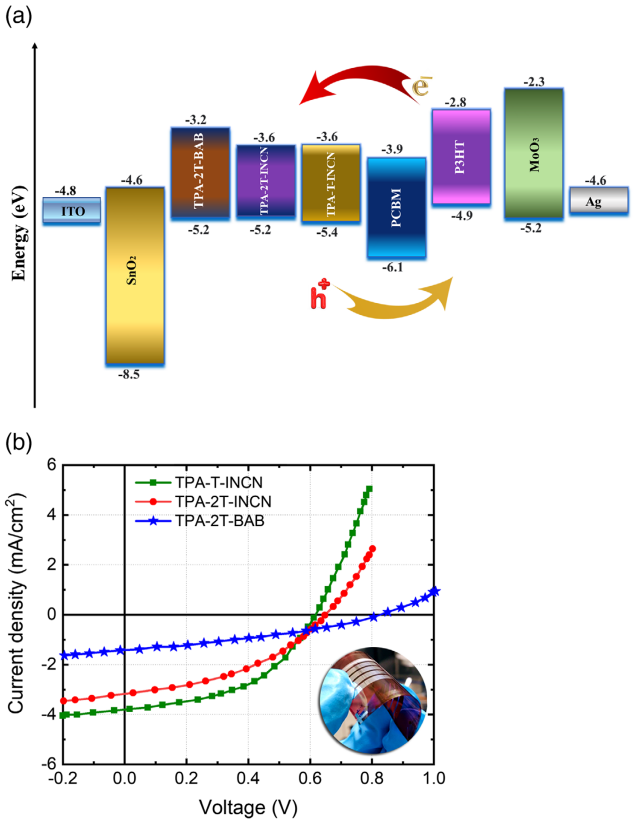

Figure 4. a) Energy band schematic diagram of the used components in OPVs. Data for ITO, SnO_2, P3HT, PCBM, MoO_3, and Ag are from the study by Huang et al.[58] HOMO and LUMO energy levels of NFAs were calculated from DPV voltammograms. b) *J*–*V* curves of champion flexible OPVs with the photo of one of our typical devices in the inset.

discussed. For the device development, the donor/acceptor ratio in the binary P3HT:NFA blend was thoroughly fine tuned to enhance the film quality (Table S1, Supporting Information). The solubility limit for TPA-T-INCN, TPA-2T-INCN, and TPA-2T-BAB into o-dichlorobenzene was 20, 10, and 20 mg mL^{-1}, respectively. In this case, TPA-T-INCN displayed the highest solubility in *o*-dichlorobenzene compared with TPA-2T-INCN, allowing us to use a higher concentration of TPA-T-INCN. As TPA-2T-INCN and TPA-2T-BAB contain two octyl side chains, beneficial for materials solubility, we may have expected that these molecules would be more soluble than TPA-T-INCN. However, as shown in Figure 2a,b, a redshift in the absorption spectra of the films of the three molecules versus their absorption in solution is noted (redshift of 10 nm for TPA-T-INCN, 70 nm for TPA-2T-INCN, and 12 nm for TPA-2T-BAB). As discussed above, this indicates a more significant aggregation for TPA-2T-INCN molecule with respect to the other two, in turn leading to poorer solubility. The current density (J) –voltage (V) curves of the champion devices based on the optimized P3HT:TPA-T-INCN (20:20 mg mL^{-1}), P3HT:TPA-2T-INCN (15:10 mg mL^{-1}), and P3HT:TPA-2T-BAB (15:10 mg mL^{-1}) blends are shown in Figure 4b. The corresponding photovoltaic parameters of the flexible OPVs are summarized in **Table 3**. First, the reference OPV comprising the P3HT:PCBM active layer (20:20 mg mL^{-1}) shows a reasonable PCE of 3.19% with an open-circuit voltage (V_{OC}) of 0.58 V, a short-circuit current density (J_{SC}) of 8.55 mA cm^{-2}, and a fill factor (FF) of 64% (Table 3, Figure S6, Supporting Information), which are in good agreement with the observed most efficient interfacial charge transfer dynamics based on our TRPL data. This performance is in agreement with the state-of-the-art P3HT:PCBM solar cells, showing PCE slightly above 3% and 4% on flexible and rigid substrates, respectively.[56,57] Among the P3HT:NFA blends, P3HT:TPA-T-INCN led to the best performance with PCE = 1.13%, V_{OC} = 0.6 V, J_{SC} = 3.82 mA cm^{-2}, and FF = 49%. The J_{SC} value (3.82 mA cm^{-2}) of TPA-T-INCN cells is 16% and 62% higher than that of TPA-2T-INCN (J_{SC} = 3.20 mA cm^{-2}) and TPA-2T-BAB (J_{SC} = 1.45 mA cm^{-2}) devices, respectively. The significantly lower J_{SC} for TPA-2T-BAB cells could be related to the optical properties of P3HT:TPA-2T-BAB, which has the widest optical bandgap (2.08 eV) and shows the narrowest absorption range among the three NFA blends (Figure 2d). This may be attributed to the overlapping of TPA-2T-BAB with the absorption area of P3HT, as shown in Figure 2d, as well as its higher optical bandgap (2.08 eV). On the other hand, the highest J_{SC} is obtained with TPA-T-INCN NFA, which has also the strongest absorption due to its highest concentration, as discussed earlier. The PL quenching and TRPL studies also support the lowest performance of the OPVs with P3HT: TPA-2T-BAB blend. Indeed, in this case, the lowest quenching efficiency and slowest electron transfer rate were achieved, which are directly related to the J_{SC}. The PL trend is consistent also for TPA-2T-INCN and TPA-T-INCN blends, with the latter leading to the highest quenching efficiency and longest average PL lifetime (and highest PCE). The PL properties can be connected to the molecular structures of the NFAs. The closest proximity of the functional groups to the central group of the INCN molecules may also result in improved intramolecular charge transport. However device based on P3HT:TPA-2T-INCN achieved the moderate performance PCE of 0.86% (V_{OC} = 0.64 V, J_{SC} = 3.20 mA cm^{-2}, and FF = 42%). P3HT:TPA-2T-BAB 15:10 mg mLbased device presents lowest PCE of 0.41% (V_{OC} = 0.82 V, J_{SC} = 1.45 mA cm^{-2}, and FF = 34%). Despite the P3HT:TPA-2T-BAB-based device showing a higher V_{OC} than other star-shaped NFA-based devices, the remarkably low J_{SC} and FF drastically reduce the PCE. Even though the P3HT:TPA-2T-BAB blend appears to provide a very high V_{OC}, due to a lower FF, the TPA-2T-BAB does not show efficient electron acceptor behavior with P3HT, and the device function is mostly resistive.

Overall, when looking at the solar cell performance, both the INCN-based NFAs appear as more promising electron acceptors than the BAB-based counterpart. The better solubility of TPA-T-INCN enables the strongest absorption and the highest J_{SC}, which is the predominant reason for the best PCE of the OPVs employing this material in the BHJ blend.

Table 3. Performance of the tested star-shaped NFAs with the optimized blend ratios (20:20 mg mL^{-1}, 15:10 mg mL^{-1}, and 15:10 mg mL^{-1} for **TPA-T-INCN**, **TPA-2T-INCN**, and **TPA-2T-BAB**, respectively).

Blend[a)]		J_{SC} [mA cm^{-2}]	V_{OC} [V]	FF [%]	PCE [%]
3HT:PCBM[b)]	Average	8.24 ± 0.35	0.58 ± 0.005	61 ± 2	2.95 ± 0.17
	Best	8.55	0.58	64	3.19
P3HT:TPA-T-INCN	Average	3.23 ± 0.41	0.61 ± 0.007	47 ± 4	0.91 ± 0.14
	Best	3.82	0.6	49	1.13
P3HT:TPA-2T-INCN	Average	2.75 ± 0.26	0.60 ± 0.032	40 ± 3	0.66 ± 0.11
	Best	3.2	0.64	42	0.86
P3HT:TPA-2T-BAB	Average	1.27 ± 0.18	0.72 ± 0.101	35 ± 4	0.32 ± 0.08
	Best	1.45	0.82	34	0.41

[a)]The optimized blend ratios of the P3HT:acceptor: 1) PCBM, 2) TPA-T-INCN, 3) TPA-2T-INCN, and 4) TPA-2T-BAB with blend ratios of 20:20, 20:20, 15:10, and 15:10 mg mL^{-1} respectively. The data in represent the average values (from 16 independent devices) with the corresponding standard deviations; [b)]Reference cell.

2.5. Surface Morphology of the Active Layers

The surface morphology of the investigated BHJ blends was studied by atomic force microscopy (AFM) to obtain high spatial resolution images. **Figure 5**a–d shows 2D images of the P3HT:acceptor blend films, with the electron acceptor being PCBM, TPA-T-INCN, TPA-2T-INCN, or TPA-2T-BAB with blend ratios of 20:20, 20:20, 15:10, and 15:10 mg mL^{-1}, respectively. The 3D projections of the same images are in Figure S7, Supporting Information. The films for AFM imaging were spin coated on silicon wafer substrates under the same conditions as for the device active layers (speed of 600 rpm followed by thermal annealing inside a nitrogen-filled glovebox at 120 °C for 10 min). It is known that the morphology of the active layer is affected by several factors, such as the type and ratio of the donors and acceptors, film processing conditions, and the device architecture. Notably, the different solubility and miscibility behavior of donor and acceptor in a single solvent, during active layer film formation, may result in different micro- and

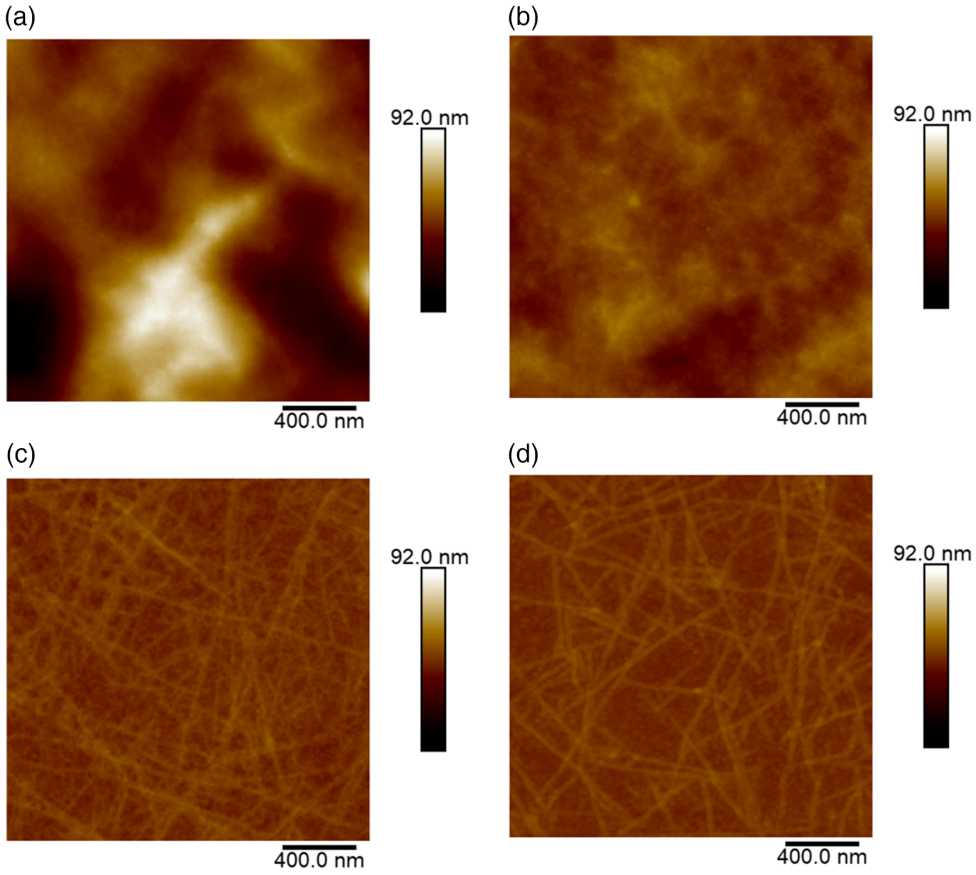

Figure 5. 2D AFM images of the P3HT:acceptor blend films: a) PCBM, b) TPA-T-INCN, c) TPA-2T-INCN, and d) TPA-2T-BAB with blend ratios of 20:20, 20:20, 15:10, and 15:10 mg mL^{-1}, respectively.

nanostructures that could affect the OPV performance. In our case, it is evident that the blends with the studied electron acceptors present a quite different texture (Figure 5), which can be also linked to their photovoltaic performance (Table 3), assuming that the detected surface morphology carries through the film. A notable difference in the blend morphology was observed between P3HT:TPA-T-INCN sample (similar to that of P3HT:PCBM) and the other two blend films (i.e., P3HT:TPA-2T-INCN and P3HT:TPA-2T-BAB), as shown in Figure 5, most probably accounting for the different performances. The moderate phase separation and more uniform distribution of P3HT:TPA-T-INCN and P3HT:PCBM films are definitely beneficial for the charge transport and lead to the highest PCE value among the three NFA-based blend films. On other hand, a fibrillar network is observed for P3HT:TPA-2T-INCN and P3HT:TPA-2T-BAB blend films, which we suspect to be caused by lower P3HT:NFA ratios and by the tendency of 2T molecules to aggregate, as hinted by the DFT study. This, in turn, is detrimental for the exciton dissociation and charge transport and results in poor device performance.[59,60]

3. Conclusion

We designed and synthesized three novel star-shaped NFA molecules based on TPA core and linked through π-conjugated thiophene spacers to different terminal units (INCN and BAB), namely, TPA-2T-INCN, TPA-2T-BAB, and TPA-T-INCN. The optical and electrochemical properties of the NFAs were investigated. When the electron-acceptors were blended with the P3HT donor polymer, the samples displayed a large difference in the PL quenching efficiency. The highest values were obtained with TPA-T-INCN and TPA-2T-INCN blends. This indicates that INCN-based NFAs possess more energetically suitable electron affinities (−3.6 eV) than BAB-based materials (−3.2 eV) for efficiently accepting the injected electrons from the LUMO level (−2.8 eV) of P3HT. Furthermore, the TRPL outcomes showed that the TPA-T-INCN indeed promotes an efficient charge extraction process while limiting the charge recombination at the interface. Furthermore, P3HT-based BHJ OPVs with TPA-T-INCN acceptor confirmed this and showed the best performance in flexible OPVs (PCE = 1.13%, FF = 49%, V_{OC} = 0.6 V, and J_{SC} 3.82 mA cm^{-2}). This was explained by both the energy level/charge transfer and the improved solubility of the TPA-T-INCN in *o*-dichlorobenzene with respect to the other NFAs. Assuming that the observed surface morphology carries through the blend films, the AFM study supports the photovoltaic results, as P3HT:TPA-T-INCN showed a more uniform distribution of P3HT and TPA-T-INCN in the blend compared to P3HT:TPA-2T-INCN, and P3HT:TPA-2T-BAB samples, for which a fibrillar network morphology was found.

Supporting Information

Supporting Information is available from the Wiley Online Library or from the author.

Acknowledgements

This work was part of the Academy of Finland Flagship Programme, Photonics Research and Innovation (PREIN), decision no. 320165.

Conflict of Interest

The authors declare no conflict of interest.

Data Availability Statement

The data that support the findings of this study are available from the corresponding author upon reasonable request.

Keywords

barbiturate, flexible photovoltaics, indene malononitrile, nonfullerene acceptors, organic photovoltaics, star-shaped acceptors

Received: March 17, 2022
Revised: May 12, 2022
Published online: June 22, 2022

[1] M. Ylikunnari, M. Välimäki, K.-L. Väisänen, T. M. Kraft, R. Sliz, G. Corso, R. Po, R. Barbieri, C. Carbonera, G. Gorni, M. Vilkman, *Flexible Printed Electron.* **2020**, *5*, 014008.
[2] M. K. Välimäki, E. Jansson, V. J. Von Morgen, M. Ylikunnari, K.-L. Väisänen, P. Ontero, M. Kehusmaa, P. Korhonen, T. M. Kraft, *Int. J. Adv. Manuf. Technol.* **2022**, *7*, 9570.
[3] M. Välimäki, P. Apilo, R. Po, E. Jansson, A. Bernardi, M. Ylikunnari, M. Vilkman, G. Corso, J. Puustinen, J. Tuominen, J. Hast, *Nanoscale* **2015**, *7*, 9570.
[4] S. Chatterjee, S. Jinnai, Y. Ie, *J. Mater. Chem. A* **2021**, *9*, 18857.
[5] S. J. Jeon, Y. H. Kim, I. N. Kim, N. G. Yang, J. H. Yun, D. K. Moon, *J. Energy Chem.* **2022**, *65*, 194.
[6] L. Dou, J. You, Z. Hong, Z. Xu, G. Li, R. A. Street, Y. Yang, *Adv. Mater.* **2013**, *25*, 6642.
[7] S.-C. Lan, P.-A. Yang, M.-J. Zhu, C.-M. Yu, J.-M. Jiang, K.-H. Wei, *Polym. Chem.* **2013**, *4*, 1132.
[8] C. Yan, S. Barlow, Z. Wang, H. Yan, A. K.-Y. Jen, S. R. Marder, X. Zhan, *Nat. Rev. Mater.* **2018**, *3*, 1.
[9] Y. Li, T. Li, Y. Lin, *Mater. Chem. Front.* **2021**, *5*, 2907.
[10] M. A. Alamoudi, J. I. Khan, Y. Firdaus, K. Wang, D. Andrienko, P. M. Beaujuge, F. Laquai, *ACS Energy Lett.* **2018**, *3*, 802.
[11] Y. Lin, P. Cheng, Y. Li, X. Zhan, *Chem. Commun.* **2012**, *48*, 4773.
[12] X. Liu, Y. Xie, H. Zhao, X. Cai, H. Wu, S.-J. Su, Y. Cao, *New J. Chem.* **2015**, *39*, 8771.
[13] A. Rananaware, A. Gupta, J. Li, A. Bilic, L. Jones, S. Bhargava, S. V. Bhosale, *Chem. Commun.* **2016**, *52*, 8522.
[14] A. Rananaware, A. Gupta, G. Kadam, D. Duc La, A. Bilic, W. Xiang, R. A. Evans, S. V. Bhosale, *Mater. Chem. Front.* **2017**, *1*, 2511.
[15] S. M. Wagalgave, S. V. Bhosale, R. S. Bhosale, A. L. Puyad, J.-Y. Chen, J.-L. Li, R. A. Evans, A. Gupta, S. V. Bhosale, *Mater. Chem. Front.* **2019**, *3*, 1231.
[16] S. Holliday, R. S. Ashraf, A. Wadsworth, D. Baran, S. A. Yousaf, C. B. Nielsen, C.-H. Tan, S. D. Dimitrov, Z. Shang, N. Gasparini, M. Alamoudi, F. Laquai, C. J. Brabec, A. Salleo, J. R. Durrant, I. Mcculloch, *Nat. Commun.* **2016**, *7*, 1.
[17] Y. Wu, H. Bai, Z. Wang, P. Cheng, S. Zhu, Y. Wang, W. Ma, X. Zhan, *Energy Environ. Sci.* **2015**, *8*, 3215.
[18] S. Holliday, R. S. Ashraf, C. B. Nielsen, M. Kirkus, J. A. Röhr, C.-H. Tan, E. Collado-Fregoso, A.-C. Knall, J. R. Durrant, J. Nelson, I. Mcculloch, *J. Am. Chem. Soc.* **2015**, *137*, 898.
[19] D. Baran, T. Kirchartz, S. Wheeler, S. Dimitrov, M. Abdelsamie, J. Gorman, R. S. Ashraf, S. Holliday, A. Wadsworth, N. Gasparini, P. Kaienburg, H. Yan, A. Amassian, C. J. Brabec, J. R. Durrant, I. Mcculloch, *Energy Environ. Sci.* **2016**, *9*, 3783.
[20] A. Aljarilla, L. López-Arroyo, P. de la Cruz, F. Oswald, T. B. Meyer, F. Langa, *Org. Lett.* **2012**, *14*, 5732.
[21] P. Gao, H. N. Tsao, M. Grätzel, M. K. Nazeeruddin, *Org. Lett.* **2012**, *14*, 4330.
[22] Z. Gu, P. Tang, B. Zhao, H. Luo, X. Guo, H. Chen, G. Yu, X. Liu, P. Shen, S. Tan, *Macromolecules* **2012**, *45*, 2359.
[23] J.-H. Kim, H. U. Kim, D. Mi, S.-H. Jin, W. S. Shin, S. C. Yoon, I.-N. Kang, D.-H. Hwang, *Macromolecules* **2012**, *45*, 2367.
[24] C. Mallet, G. Savitha, M. Allain, V. Kozmík, J. Svoboda, P. Frère, J. Roncali, *J. Org. Chem.* **2012**, *77*, 2041.
[25] N. Metri, X. Sallenave, C. Plesse, L. Beouch, P.-H. Aubert, F. Goubard, C. Chevrot, G. Sini, *J. Phys. Chem. C* **2012**, *116*, 3765.
[26] G. Kadam, A. Anuradha, A. Agarwal, A. Puyad, D. D. La, R. A. Evans, J. Li, A. Gupta, S. V. Bhosale, *Mater. Chem. Front.* **2018**, *2*, 1090.
[27] R. W. Jadhav, R. V. Hangarge, M. D. Aljabri, K. S. More, J.-Y. Chen, L. A. Jones, R. A. Evans, J.-L. Li, S. V. Bhosale, A. Gupta, *Mater. Chem. Front.* **2020**, *4*, 2176.
[28] A. K. Hundal, S. Ali, M. Jameel, L. Jones, N. Kaur, R. A. Evans, J.-L. Li, S. J. Langford, A. Gupta, *Mater. Chem. Front.* **2020**, *4*, 3209.
[29] Y.-Q. Pan, G.-Y. Sun, *ChemSusChem* **2019**, *12*, 4570.
[30] M. U. Khan, M. Khalid, M. N. Arshad, M. N. Khan, M. Usman, A. Ali, B. Saifullah, *ACS Omega* **2020**, *5*, 23039.
[31] M. U. Khan, M. Y. Mehboob, R. Hussain, R. Fatima, M. S. Tahir, M. Khalid, A. A. C. Braga, *J. Phys. Org. Chem.* **2021**, *34*, e4119.
[32] Y. Shirota, *J. Mater. Chem.* **2005**, *15*, 75.
[33] Y. Lin, Y. Li, X. Zhan, *Chem. Soc. Rev.* **2012**, *41*, 4245.
[34] A. Tang, L. Li, Z. Lu, J. Huang, H. Jia, C. Zhan, Z. Tan, Y. Li, J. Yao, *J. Mater. Chem. A* **2013**, *1*, 5747.
[35] Y. N. Luponosov, A. N. Solodukhin, A. L. Mannanov, P. S. Savchenko, B.A. L. Raul, S. M. Peregudova, N. M. Surin, A. V. Bakirov, M. A. Shcherbina, S. N. Chvalun, M. S. Pshenichnikov, D. Y. Paraschuk, S. A. Ponomarenko, *Mater. Today Energy* **2021**, *22*, 100863.
[36] Y. Lin, J. Wang, Z.-G. Zhang, H. Bai, Y. Li, D. Zhu, X. Zhan, *Adv. Mater.* **2015**, *27*, 1170.
[37] Y. Zhou, M. Li, H. Lu, H. Jin, X. Wang, Y. Zhang, S. Shen, Z. Ma, J. Song, Z. Bo, *Adv. Funct. Mater.* **2021**, *31*, 2101742.
[38] J.-C. Choe, T. H. Lee, E. Lim, *Bull. Korean Chem. Soc.* **2019**, *40*, 20.
[39] P. Sullivan, G. E. Collis, L. A. Rochford, J. F. Arantes, P. Kemppinen, T. S. Jones, K. N. Winzenberg, *Chem. Commun.* **2015**, *51*, 6222.
[40] J. Zhang, D. Deng, C. He, Y. He, M. Zhang, Z.-G. Zhang, Z. Zhang, Y. Li, *Chem. Mater.* **2011**, *23*, 817.
[41] J. Min, Y. N. Luponosov, D. Baran, S. N. Chvalun, M. A. Shcherbina, A. V. Bakirov, P. V. Dmitryakov, S. M. Peregudova, N. Kausch-Busies, S. A. Ponomarenko, T. Ameri, C. J. Brabec, *J. Mater. Chem. A* **2014**, *2*, 16135.
[42] H. M. Diab, A. M. Abdelmoniem, M. R. Shaaban, I. A. Abdelhamid, A. H. M. Elwahy, *RSC Adv.* **2019**, *9*, 16606.
[43] Y. Xie, L. Ye, Y. Cai, X. Zhang, J. Xu, T. Wang, F. Liu, Y. Sun, *Small Struct.* **2021**, *2*, 2100055.

[44] C. Zhu, A. J. Kalin, L. Fang, *Acc. Chem. Res.* **2019**, *52*, 1089.
[45] S. Pang, X. Zhou, S. Zhang, H. Tang, S. Dhakal, X. Gu, C. Duan, F. Huang, Y. Cao, *ACS Appl. Mater. Interfaces* **2020**, *12*, 16531.
[46] J. Hou, O. Inganäs, R. H. Friend, F. Gao, *Nat. Mater.* **2018**, *17*, 119.
[47] G. P. Kini, H. S. Park, S. J. Jeon, Y. W. Han, D. K. Moon, *Sol. Energy* **2020**, *207*, 720.
[48] C. Zhan, J. Yao, *Chem. Mater.* **2016**, *28*, 1948.
[49] R. Li, Z. Dai, M. Zheng, C. Wang, Z. Deng, T. Zhuang, K. Feng, W. Yang, K. Yang, H. Zhang, *Macromol. Rapid Commun.* **2021**, *42*, 2000703.
[50] M. Schubert, D. Dolfen, J. Frisch, S. Roland, R. Steyrleuthner, B. Stiller, Z. Chen, U. Scherf, N. Koch, A. Facchetti, D. Neher, *Adv. Mater.* **2012**, *2*, 369.
[51] N. D. Eastham, A. S. Dudnik, T. J. Aldrich, E. F. Manley, T. J. Fauvell, P. E. Hartnett, M. R. Wasielewski, L. X. Chen, F. S. Melkonyan, A. Facchetti, R. P. H. Chang, T. J. Marks, *Chem. Mater.* **2017**, *29*, 4432.
[52] M. Shirvani, L. Naji, *Mater. Chem. Phys.* **2021**, *259*, 124064.
[53] S. Grankowska Ciechanowicz, K. P. Korona, A. Wolos, A. Drabinska, A. Iwan, I. Tazbir, J. Wojtkiewicz, M. Kaminska, *J. Phys. Chem. C* **2016**, *120*, 11415.
[54] X. Yang, M. Niu, P. Bi, Z. Chen, J. Liu, X. Hao, *J. Phys. Chem. C* **2018**, *122*, 9843.
[55] C. Yang, S. Zhang, J. Ren, M. Gao, P. Bi, L. Ye, J. Hou, *Energy Environ. Sci.* **2020**, *13*, 2864.
[56] T. Stubhan, M. Salinas, A. Ebel, F. C. Krebs, A. Hirsch, M. Halik, C. J. Brabec, *Adv. Mater.* **2012**, *2*, 532.
[57] M. Abdallaoui, N. Sengouga, A. Chala, A. Meftah, A. Meftah, *Opt. Mater.* **2020**, *105*, 109916.
[58] S. Huang, Y. Tang, A. Yu, Y. Wang, S. Shen, B. Kang, S. R. P. Silva, G. Lu, *Org. Electron.* **2018**, *62*, 373.
[59] F. Zhao, C. Wang, X. Zhan, *Adv. Mater.* **2018**, *8*, 1703147.
[60] S. Bao, H. Yang, H. Fan, J. Zhang, Z. Wei, C. Cui, Y. Li, *Adv. Mater.* **2021**, *33*, 2105301.